Expanded View Figures

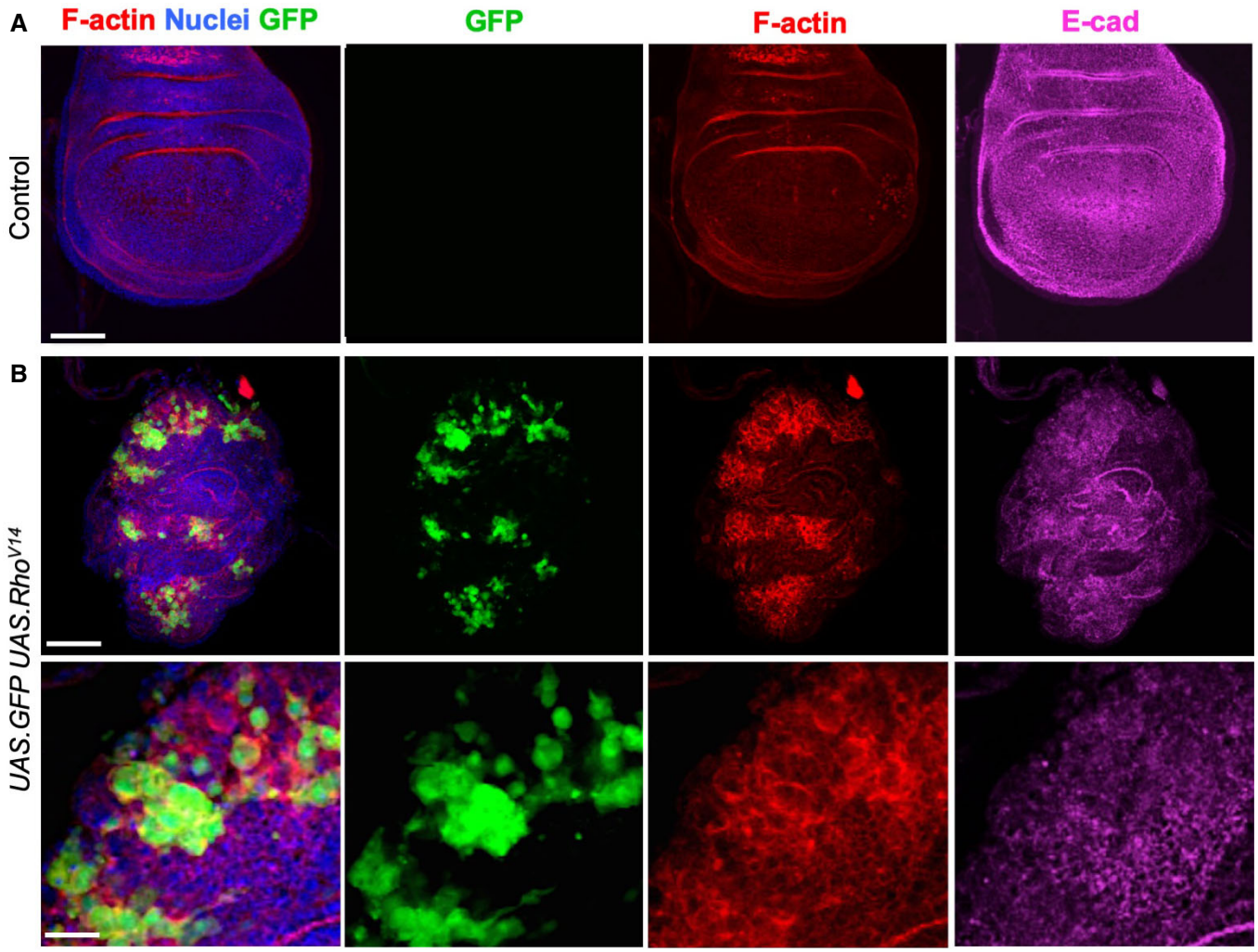

Figure EV1. Ectopic activation of Rho is sufficient to drive cell rounding and downregulate adherens junctions in the *Drosophila* wing disc.

A Control third instar wing imaginal disc stained for F-actin (phalloidin, red) and E-cadherin (magenta). Note absence of clones (GFP), there is no background signal for GFP. Scale bar ~20 μm. $n > 4$ independent biological replicates.

B Induction of clones expressing *UAS.GFP* and *UAS.RhoV14* causes dramatic increases in F-actin and co-incident decreases in E-cadherin, along with abnormal tissue morphology. High-magnification view (bottom) shows reduced E-cadherin and rounded shape of cells expressing RhoV14. Scale bars ~20 μm (low mag) ~10 μm (high mag). $n > 4$ independent biological replicates.

Figure EV2. RNAi of ECT2/Pbl leads to enlarged cells (cytokinesis defect) or extrusion of cells from the epithelium and subsequent apoptosis (spindle orientation defect) in the *Drosophila* wing disc.

A Third instar wing imaginal disc expressing *UAS.Pbl-RNAi* in the posterior compartment driven by the *hh.Gal4* line. Note enlarged cells (marked by F-actin, aPKC or Dlg staining). DAPI marks nuclei. Scale bars ~20 μm (low mag) ~5 μm (high mag). $n > 6$ independent biological replicates.

B Third instar wing imaginal disc expressing *UAS.Pbl-RNAi* in the entire wing pouch driven by the *MS1096.Gal4* line. Note many extruded cells (marked by F-actin, aPKC or Dlg staining). DAPI marks nuclei, including many pyknotic nuclei due to apoptosis. Scale bars ~20 μm (low mag) ~5 μm (high mag). $n > 7$ independent biological replicates.

C Control cross-section of wild-type third instar wing disc stained for aPKC, Dlg and nuclei (DAPI). Scale bar ~2 μm. $n > 4$ independent biological replicates.

D Cross-section of third instar wing imaginal disc expressing *UAS.Pbl-RNAi* in the entire wing pouch driven by the *MS1096.Gal4* line. Note extrusion of cells (revealed by staining for aPKC, Dlg) and many pyknotic nuclei (DAPI staining). Arrow shows residual polarised apical domains in cells that have been extruded. Scale bar ~2 μm. $n > 9$ independent biological replicates.

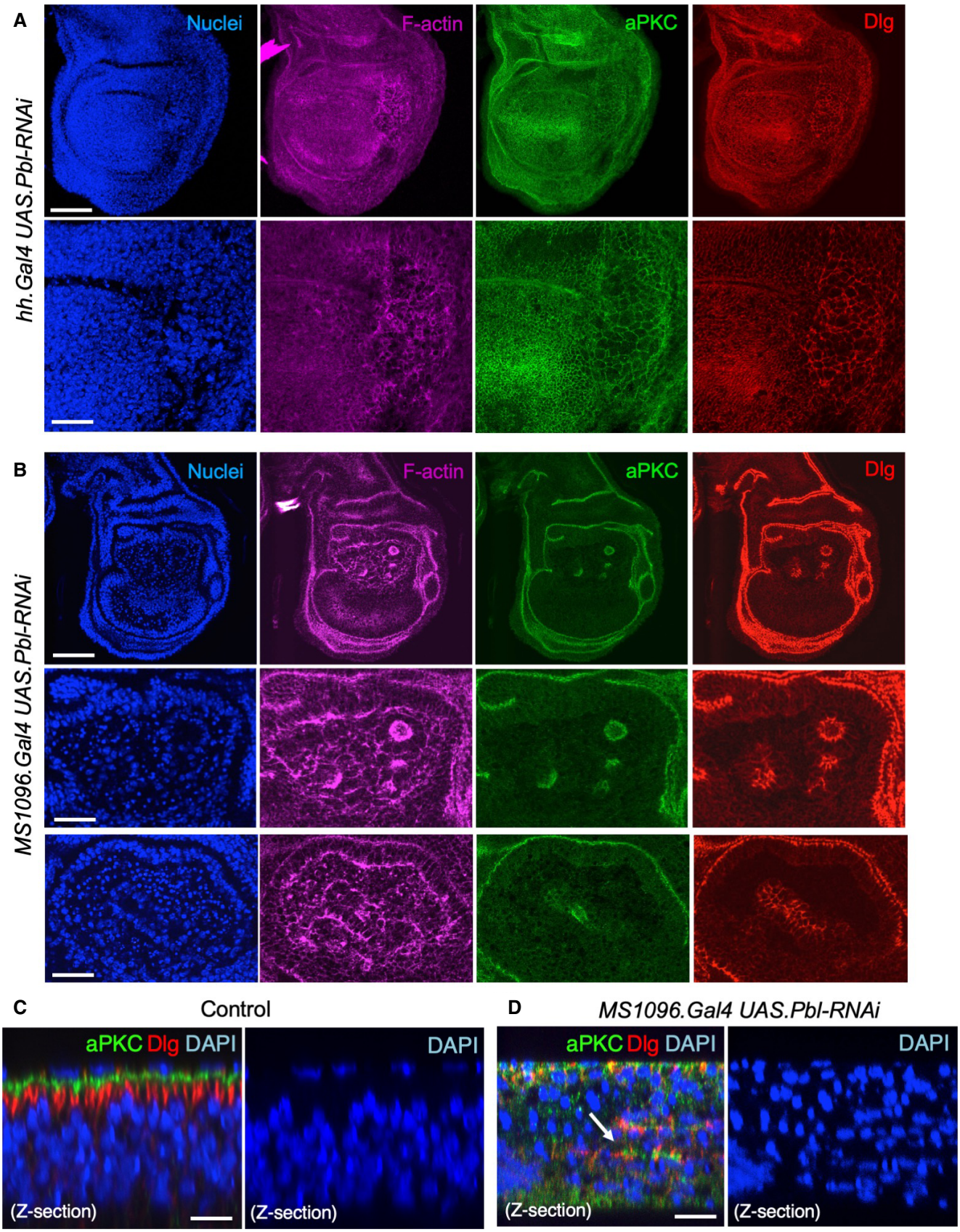

Figure EV2.

Figure EV3. RNAi of both ECT2/Pbl and beta-Pix leads to reduced apical aPKC immunostaining in the *Drosophila* follicle cell epithelium.

A Cross-section of cuboidal follicular epithelium showing cytoplasmic localisation of overexpressed Cdc42 GEF beta-PIX tagged with HA. Scale bar ~3 μm. $n > 4$ independent biological replicates.

B Cross-section of cuboidal follicular epithelium showing nuclear and cytoplasmic localisation of overexpressed ECT2/Pbl tagged with HA. Scale bar ~3 μm. $n > 10$ independent biological replicates.

C Stage 7 egg chamber in which follicle cells have mutant clones for pix^{P1036}, marked by expression of GFP, shows extrusion of cells which retain abnormal aPKC and E-cad localisation. Scale bar ~6 μm. $n > 4$ independent biological replicates.

D Stage 7 egg chamber in which follicle cells have mutant clones for pix^{P1036} also expressing *UAS.Pbl-RNAi*, marked by expression of GFP, shows extrusion of cells featuring loss of aPKC plasma membrane localisation, along with abnormal E-cad localisation. Scale bar ~6 μm. $n > 3$ independent biological replicates.

E Stage 7 egg chamber in which follicle cells have mutant clones for pix^{P1036} also expressing *UAS.Pbl-RNAi*, marked by expression of GFP, shows extrusion of cells featuring mislocalisation of p-MyoII (p-MLC), along with abnormal E-cad localisation. Scale bar ~6 μm. $n > 3$ independent biological replicates.

F High-magnification view of mutant clones for pix^{P1036} also expressing *UAS.Pbl-RNAi*, marked by expression of GFP, shows extrusion of cells featuring mislocalisation of p-MyoII (p-MLC). Scale bar ~3 μm. $n > 3$ independent biological replicates.

G Wild-type stage 7 egg chamber in which follicle cells have normal aPKC and Dlg localisation. Scale bar ~6 μm. $n > 4$ independent biological replicates.

H *tj.Gal4*-driven *UAS.pix-RNAi* causes mild extrusion of cells with abnormal aPKC localisation (arrow). Scale bar ~6 μm. $n > 5$ independent biological replicates.

I *tj.Gal4*-driven *UAS.pbl-RNAi* causes enlarged cells with normal morphology and aPKC localisation. Scale bar ~6 μm. $n > 3$ independent biological replicates.

J *tj.Gal4*-driven *UAS.pix-RNAi* and *UAS.pbl-RNAi* causes loss of aPKC throughout the follicular epithelium, while Dlg spreads ectopically. Scale bar ~6 μm. $n > 9$ independent biological replicates.

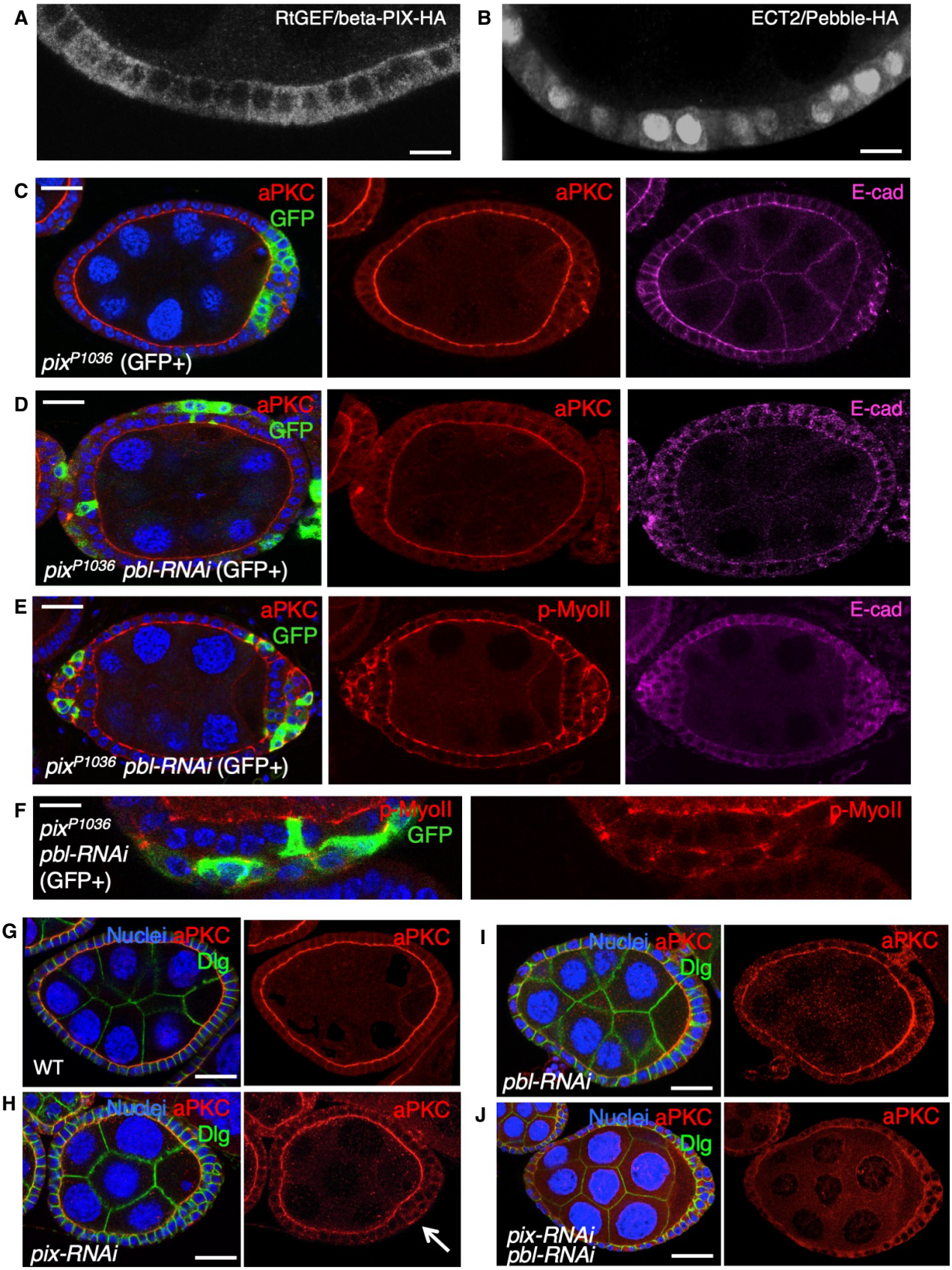

Figure EV3.

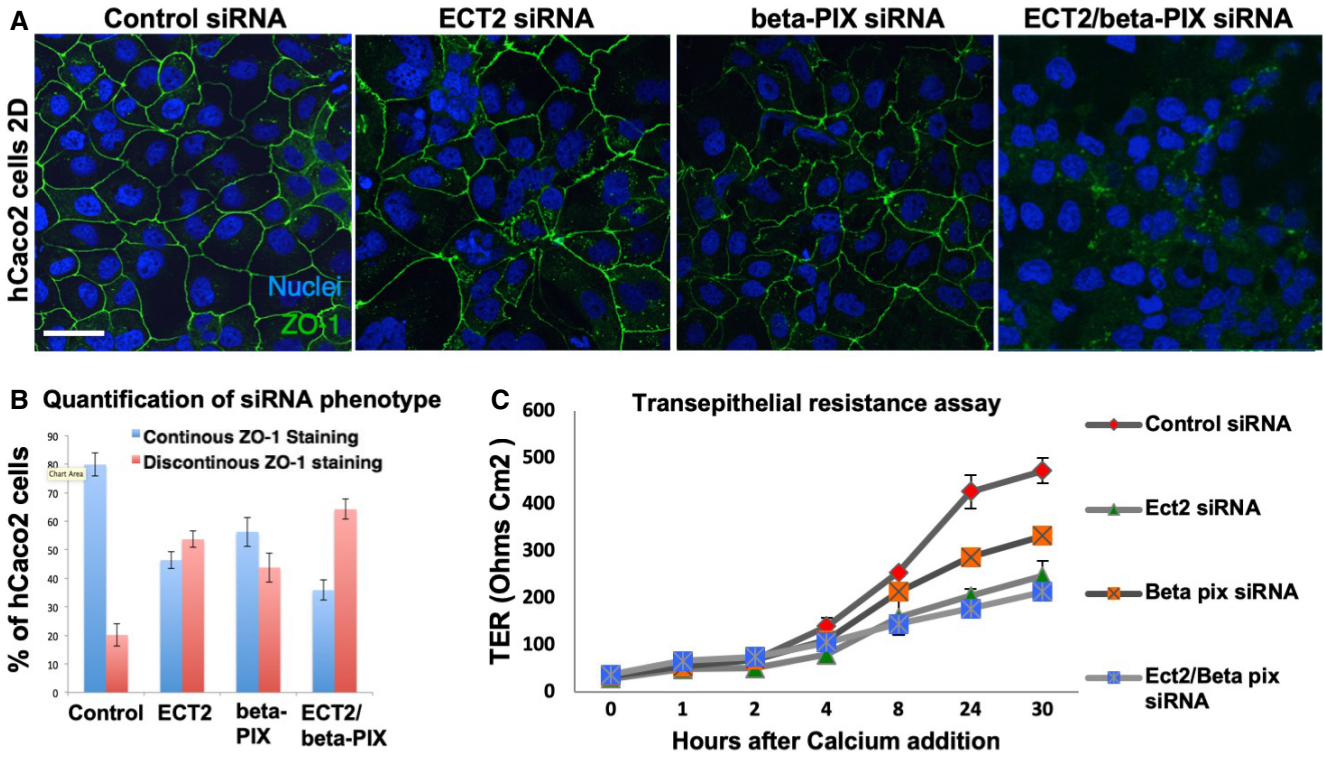

Figure EV4. RNAi of both ECT2/Pbl and beta-Pix leads to reduced apical ZO-1 immunostaining in human Caco2 cells.

A siRNA knockdown of ECT2 and beta-PIX individually does not affect the localisation of ZO-1, while double siRNA causes discontinuous ZO-1 localisation in most cells. Scale bar ~10 μm. $n > 3$ independent biological replicates.

B Quantification of (A). $n > 3$ independent biological replicates. Mean ± SEM shown.

C Transepithelial resistance assay for measuring tight junction function in each of the siRNA conditions in (A). $n > 3$ independent biological replicates. Mean ± SEM shown.

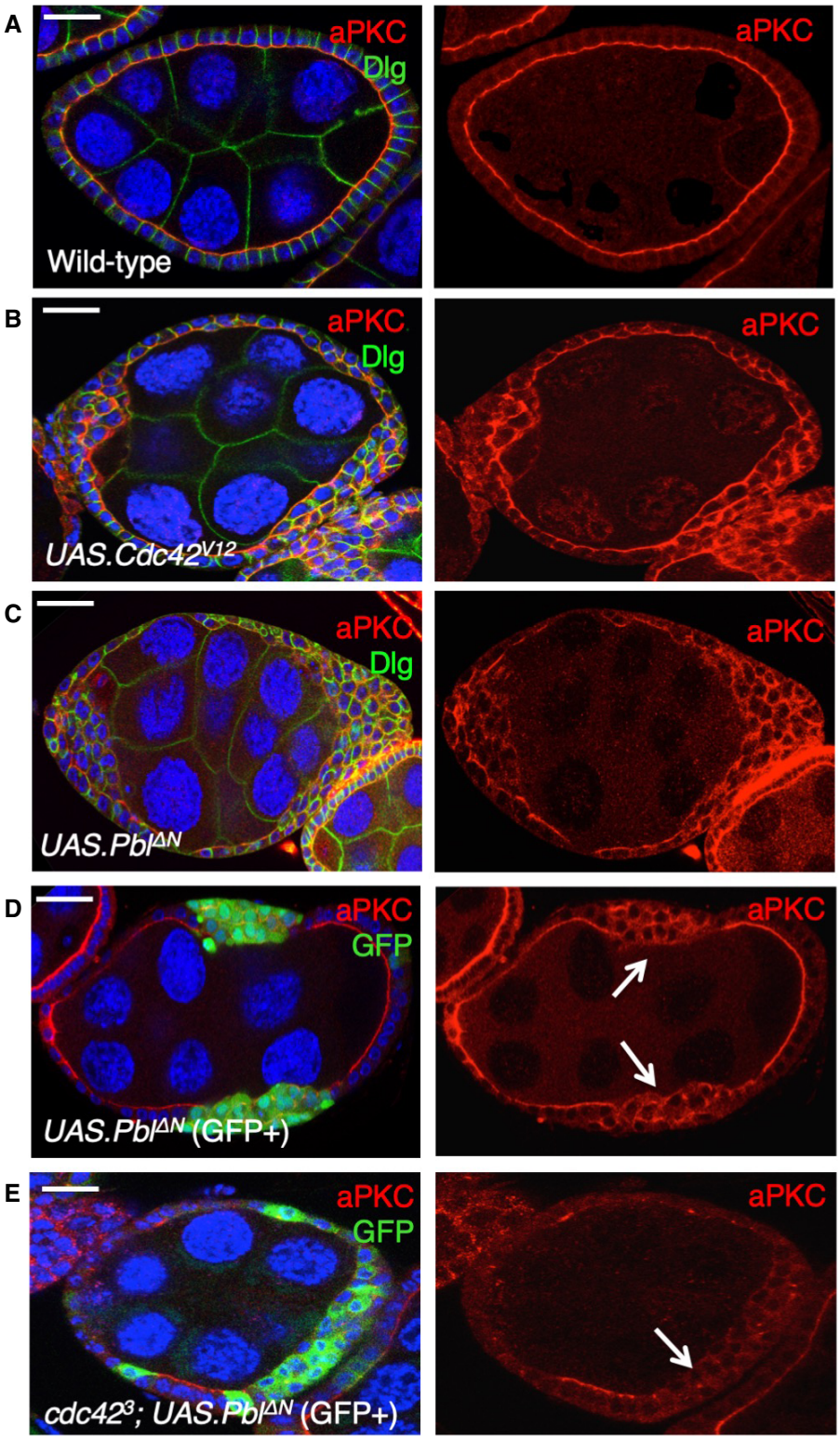

Figure EV5. Overexpression of ECT2/Pbl leads to Cdc42-dependent ectopic spreading of aPKC and cell rounding in the *Drosophila* follicle cell epithelium.

A Wild-type stage 7 egg chamber showing normal localisation of aPKC and Dlg in the follicle cell epithelium. Scale bar ~6 μm. $n > 4$ independent biological replicates.

B *tj.Gal4*-driven *UAS.Cdc42^{V12}* causes ectopic spreading of aPKC in most cells. Scale bar ~6 μm. $n > 3$ independent biological replicates.

C *tj.Gal4*-driven *UAS.Pbl-deltaN* causes ectopic spreading of aPKC in most cells. Scale bar ~6 μm. $n > 6$ independent biological replicates.

D MARCM clonal induction of *UAS.Pbl-deltaN* and *UAS.GFP* causes ectopic spreading of aPKC in most GFP-positive cells. Scale bar ~6 μm. $n > 5$ independent biological replicates. Arrows point to GFP$^+$ clones.

E MARCM induction of *UAS.Pbl-deltaN* and *UAS.GFP* in *cdc42^3* mutant clones causes loss of aPKC in most GFP-positive cells. This result indicates that overexpressed Pbl acts upstream of Cdc42 to control aPKC localisation. Scale bar ~6 μm. $n > 3$ independent biological replicates. Arrows point to GFP$^+$ clones.

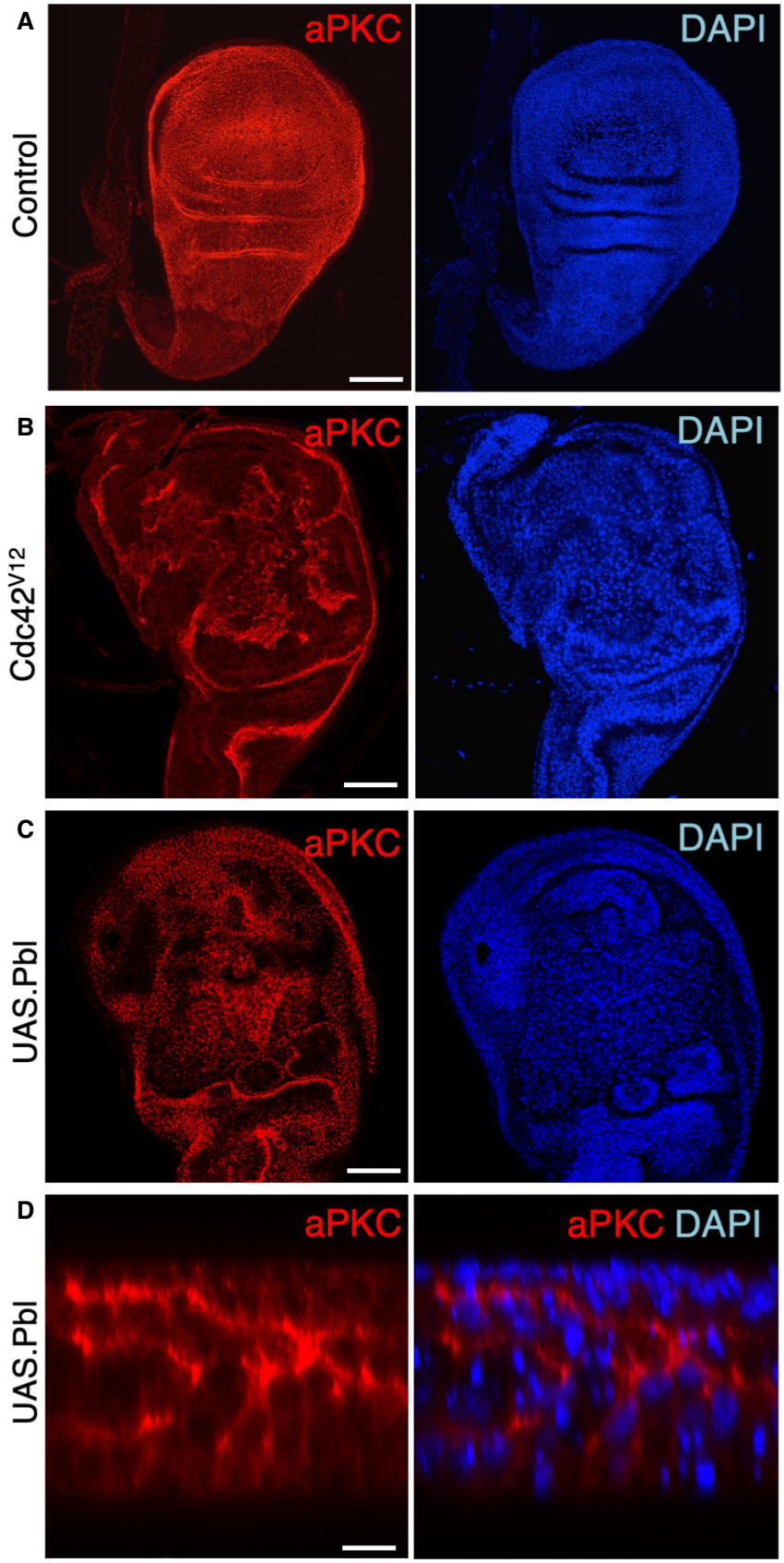

Figure EV6. Overexpression of ECT2/Pbl in the wing imaginal disc leads to ectopic spreading of aPKC and cell rounding in the *Drosophila* wing disc.

A Control third instar wing disc stained for aPKC and nuclei (DAPI). Scale bar ~20 μm. $n > 3$ independent biological replicates.

B *MS1096.Gal4*-driven *UAS.Cdc42^{V12}* causes ectopic spreading of aPKC and abnormal tissue morphology. Scale bar ~20 μm. $n > 6$ independent biological replicates.

C *MS1096.Gal4*-driven *UAS.Pbl* causes ectopic spreading of aPKC and abnormal tissue morphology. Scale bar ~20 μm. $n > 8$ independent biological replicates.

D High-magnification cross-section of *MS1096.Gal4*-driven *UAS.Pbl* causing ectopic spreading of aPKC and abnormal tissue morphology. The phenotypes of Cdc42 and Pbl gain of function are similar in the wing disc. Scale bar ~2 μm. $n > 4$ independent biological replicates.